Journal of
Marine Science and Engineering

MDPI

Article

An Investigation of the Effect of Utilizing Solidified Soil as Scour Protection for Offshore Wind Turbine Foundations via a Simplified Scour Resistance Test

Jing Wang [1], Jinbo Xie [1], Yingjie Wu [2,*], Chen Wang [2] and Fayun Liang [2]

[1] CCCC Third Harbor Engineering Co., Ltd., Shanghai 200032, China
[2] Department of Geotechnical Engineering, Tongji University, Shanghai 200092, China
* Correspondence: jacobmail@tongji.edu.cn

Abstract: Offshore wind power is rapidly developing as a source of clean energy. However, as local scour of the foundation of an offshore wind turbine can create serious safety risks to the normal operation of the turbine, it is necessary to protect the foundation from scour. In this paper, a new scour protection countermeasure using solidified soil has been investigated via an updated apparatus for a simplified scour resistance test (SSRT). Two types of tests were carried out: an unconfined compressive test to determine geotechnical parameters and an SSRT test to reflect the scour resistance of the soil samples. The results show that unconfined strength is approximately related to the critical flow velocity of the scour resistance as a power function. Soil samples having an unconfined compressive strength of 300 kPa can resist erosion under flow conditions above 3.14 m/s after solidification. In addition, the solidification state of the solidified soil has a great impact on the scour resistance of the soil sample, and the critical scour velocity of the final solidified soil is increased by 80–150% as compared to an initial solidified soil having the same final unconfined strength. These results suggest that attention should be paid to the state of the solidified soil during the construction process. The engineers should control the ratio of cement, water, and soil of the solidified soil according to the hydraulic parameters at the time of construction so that no great loss of solidified soil will occur during the construction process.

Keywords: scour protection; solidified soil; scour resistance; offshore wind turbine

check for updates

Citation: Wang, J.; Xie, J.; Wu, Y.; Wang, C.; Liang, F. An Investigation of the Effect of Utilizing Solidified Soil as Scour Protection for Offshore Wind Turbine Foundations via a Simplified Scour Resistance Test. *J. Mar. Sci. Eng.* **2022**, *10*, 1317. https://doi.org/10.3390/jmse10091317

Academic Editor: Eva Loukogeorgaki

Received: 15 August 2022
Accepted: 12 September 2022
Published: 17 September 2022

1. Introduction

Rapid growth in economic conditions will generally lead to a rise in the demand for energy, and the use of fossil energy sources (including oil, coal, and natural gas) results in environmental pollution issues, such as smog, acid rain, and the greenhouse effect. Nowadays, more attention has been paid to clean renewable energy due to issues with traditional fossil energy sources and their environmental effects. In this context, the number of constructed offshore wind turbines (OWTs) has grown significantly during recent decades, as shown in Figure 1 [1,2]. Offshore wind farm projects originated in Europe and have been built on a large scale in China since 2016. The Compound Annual Growth Rate (CAGR) of offshore wind power in use has increased by 47.4% from 2017 to 2021. It should be noted that since the cost of the foundation usually accounts for 20–35% of the total investment in OWTs [3], the safety and long-term service of the foundations play an important role in the development of offshore wind turbine farms.

Marine structures as well as their supportive systems will be inevitably confronted with the risk of failure due to scour, which is a natural phenomenon where sediments are removed and transported around obstructions due to the flow of water [4]. With the development of this process, scour holes form around the underwater foundations that can compromise the integrity of the superstructures and may cause failures [5]. Investigations of the scour process were first conducted in the field of bridge engineering, and significant

studies have been carried out to evaluate the influence of scour on the bearing capacity of bridge support systems [6–10]. Scour countermeasures are usually adopted to protect bridge foundations, and these protection methods can be divided into two broad categories: passive countermeasures and active countermeasures [4]. Passive countermeasures enable scour reduction by improving the scour resistance of bed materials through the use of a physical barrier, such as riprap, gabions, and blocks. In contrast, active scour countermeasures are designed to decrease the strength of the oncoming flow to reduce the erosive force generated in the local flow field, including the utilization of sacrificial piles, slots, collars, and other structures.

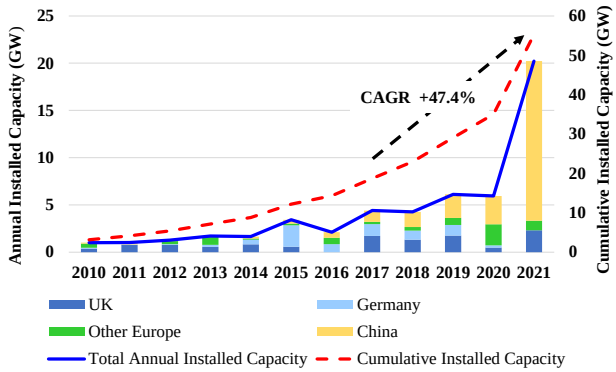

Figure 1. Annual installed offshore wind capacity (left axis) and cumulative capacity in GW (right axis) by country from 2010 to 2021.

Riprap protection and its derivative methods are the most widely used in bridge engineering because of their convenience during construction. However, changing hydraulic conditions (especially floods) may destroy riprap systems and necessitate costly repairs. Chiew [11] summarized the mechanisms of shear damage, subsidence damage, and edge damage to riprap protection systems under clear water scour conditions based on experiments; some scholars have also conducted relevant studies around this protection technology and have proposed various design formulas [12,13]. Esteban et al. [14] compared the applicability of the formulations proposed by Isbash [15], Soulsby [13], and De Vos [12] for the design of riprap protection with field data from several offshore wind farms, and they noted that the design of riprap protection should be based more on the results from laboratory studies.

The situation for OWTs confronted with scour may be quite different than those for bridges, as their superstructures are different from bridges in ways that can result in a system that will be more sensitive to scour. As scour can change the buried depth of the foundation, it not only has a great effect on the bearing capacity of an OWT but also its natural frequency. Moreover, a scoured foundation tends to cause tilting of the wind turbine superstructure, which will lead to the shutdown of an OWT once the incline reaches 5° [3]. A tilt angle tolerance value of 0.5° to 0.75° for normal operation of fans is included in DNV specifications [16]. As OWTs are located in more complex marine environments that expose them to currents as well as the action of waves, Sumer et al. [17], Myrhaug and Ong [18], and Corvaro et al. [19] explored the mechanism of scour under wave conditions and proposed or modified the corresponding scour prediction equations. The results of flume tests by Sumer and Fredsøe [20] and Chen et al. [21] showed that the combined effect of waves and currents can significantly accelerate the development of scour. Qi and Gao [22] found that the scour depth when the foundation reaches equilibrium under the combined action of waves and currents is greater than the linear sum of the two when considered separately. Hence, the selection of a proper protective method is important for structural safety and cost savings, otherwise the final price of the generated power will be uncompetitive. Furthermore, to avoid changing the natural frequency of the entire structure, it is not recommended to install countermeasures directly on the foundation. Thus, improving the scour resistance of the bed materials can be a good alternative. In

the early years of offshore wind farm construction, special considerations were not made for scour protection of the foundations of OWTs, and the solutions were mainly based on those used in bridge engineering: riprap protection, concrete chain row, sandbags (sand quilts), and so on. However, due to differences in the conditions and influences of scour for OWTs and bridges, deficiencies have been shown in practice when using these methods for OWTs [17,23]. For this reason, engineers and researchers are making efforts to find a protective method that is reliable for OWTs.

Soil reinforcement technology has been widely used in slope and bank protection to improve the soil properties and increase the soil strength and water stability, which can effectively enhance the ability of the slope or bank to resist external loads and environmental changes. Zhang et al. [24] investigated the strength characteristics of clay soils with high water content that were solidified by low-dosage cement, and they proposed an empirical formula for strength versus water content, soil-to-cement ratio, and maintenance pressure. Li [25] studied the solidified formulation for Hangzhou marine soils and established a strength change model as well as an elastic–plastic damage model for the solidified soils. In the study of solidified soil materials, the combination of cement and silty clay has been of interest to many researchers [24,26–28]. With the increase in restrictions due to environmental protection policies, the mining of sand and gravel materials for riprap and sandbag protection has been limited; in contrast, the concept of soil reinforcement shows great potential in scour protection.

Considering the convenience of using this technology during construction, attempts have been made to use cement-solidified soils for scour protection around offshore wind turbines. However, the specifications for soil solidification in marine engineering are not as sophisticated as those for projects on land [29]. Research on the mechanism of solidified soils used for scour protection is still limited, and it cannot meet the requirements of engineering practice. During the service life of constructed OWTs, inspections must be conducted frequently by personnel on engineering vessels, especially after extreme conditions, such as windstorms. This brings a heavy economic burden when unnecessary checks must be made (resulting in costs in the range of hundreds of thousands of dollars each time a farm must be checked) or creates a potential risk when a critical check is missed. Therefore, investigations on the use of cement-solidified soils as scour countermeasures are in significant demand by OWTs designers.

The research on scour can be divided into macroscopic and microscopic mechanisms based on the different emphases and testing methods [4]. The former mainly simulates the development of scour around foundation models under different flow conditions, compares the development of scour depth over time by large- or field-scale experiments, and analyses the influence of macroscopic parameters (including flow speed, wavelength, period, and other factors) on the scour results. In contrast, microscopic study primarily treats the samples as a small unit, focuses on the process of water–soil interaction, and compares the factors affecting the initiation of soil surface erosion [30,31]. At a microscopic level, the development of scour can be regarded as the continuous erosion of the bed materials. Scour initiates when the soils are eroded due to the local flow field, including horseshoe vortices and downward flow. The critical shear stress, τ_c, is an important parameter that can be used to judge the occurrence of erosion. When the shear stress caused by the flow is lower than the critical shear stress, erosion will not occur. Briaud [30] tested the scour resistance of sand using an erosion function apparatus (EFA) and suggested that the critical shear stress of the sand is related to and numerically equal to the median grain size of the sand. In a flume experiment, Maniatis et al. [32] investigated the pebble transport mechanism at a fine scale by implanting a micro-electromechanical system in the pebbles to monitor the acceleration and the force to which the pebbles are subjected during erosion. Li et al. [33] used a computational fluid dynamics/discrete element method (CFD-DEM) coupled numerical model to analyze the erosion forces and trajectories of soil particles around the foundation in the local scour of a bridge. The authors have proposed using the simplified scour resistance test (SSRT) to evaluate the scour resistance of the soil samples.

From an engineering perspective, however, it is still not easy to use these test methods due to their complicated operation and high costs. At the same time, an unconfined compression test is relatively simple and is commonly used in engineering practice. Once the relationship between the geotechnical indices (namely the unconfined compressive strength, UCS), and the scour resistance of the materials has been established, it can be convenient for engineers to evaluate the scour characteristics of cement-solidified soils for the purpose of using them as scour countermeasures.

The purpose of this study is to explore the microscopic mechanisms of cement-solidified soils and to establish the relationship between the scour characteristics of the solidified soil and its unconfined compressive strength. Based on the results of laboratory tests, recommendations for the design of scour countermeasures using cement-solidified soils are provided. The relationship between the UCS of cemented solidified soil and the soil-to-cement ratio was first established by using the unconfined compression test. After determining the soil-to-cement ratio and the water-to-cement ratio, the critical scour flow velocity, equilibrium erosion depth, and equilibrium erosion volume of the solidified soil with different unconfined compressive strengths were tested by SSRT to measure the scour resistance of the solidified soil. An analysis of the test results and some recommendations based on the test results are also provided.

2. Mechanism of Scour and Scour Protection

2.1. Scour around Underwater Foundations

As shown in Figure 2, the scour around an offshore wind power foundation is a result of the interaction between the current, the soil, and the structure. When the current reaches the vicinity of the foundation, a more complex local flow field is generated around the foundation (see Figure 2) that can be roughly divided into a downflow, a horseshoe vortex, and a wake vortex [31]. When subjected to these flow patterns, sand particles exhibit two typical erosion processes, sliding and rolling, with three possible outcomes for the eroded particles: (1) particles are carried by the flow of water and are deposited at a location downstream once the flow velocity becomes low enough; (2) particles will roll on the soil bed from their starting position until they become stabilized at a point downstream; and (3) particles slide into an adjacent scour pit. For clay, the erosion of particles tends to occur in clusters [34].

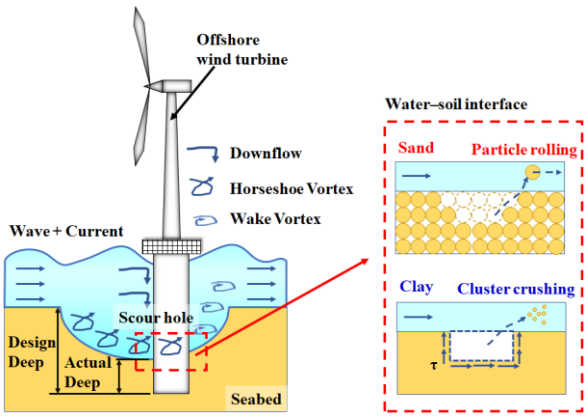

Figure 2. Schematic diagram of the scour mechanism for an OWT.

When exposed to the combined effects of water flow, foundation, and soil, scour will occur when the scour effect on the soil around the foundation is greater than its scour resistance. The scour effect is usually characterized by the flow velocity (V) or the shear force (τ) generated by the flow of water on the soil, which is influenced by the flow parameters (flow velocity v_w) and the foundation parameters (pile radius D), while the scour resistance of the soil (critical flow velocity V_c or critical shear stress τ_c) is influenced

by the geotechnical parameters of the soil itself (the median particle size d_{50}, cohesion c, etc.). The occurrence of the scour phenomenon can be determined using the following equation:

$$\tau(v_w, D) > \tau_c(d_{50}, c, \ldots) \quad or \quad V(v_w, D) > V_c(d_{50}, c, \ldots) \tag{1}$$

Because the foundation of the wind turbine is located in a marine environment, the shear stress acting on the protective layer should usually consider the combined effect of currents and waves. Equation (2), which is provided by Soulsby [12], is a method for calculating shear stress considering the combined action of current and waves.

$$\begin{aligned} \tau_{\mathrm{wcmax}} &= \left[(\tau_{\mathrm{m}} + \tau_{\mathrm{w}} \cos\phi)^2 + (\tau_{\mathrm{w}} \sin\phi)^2\right]^{1/2} \\ \tau_{\mathrm{m}} &= \tau_c \left[1 + 1.2\left(\frac{\tau_{\mathrm{w}}}{\tau_c + \tau_{\mathrm{w}}}\right)^{3.2}\right] \end{aligned} \tag{2}$$

where τ_{m} is the mean combined bed shear stress, τ_{w} is the wave-induced bed shear stress, τ_c is the current-induced bed shear stress, and ϕ is the angle between the wave and the current.

In the DNV specification [16], an equation to calculate the maximum flow velocity at the bottom of the approaching water under the combined action of wave flow is also proposed as shown in Equation (3)

$$\begin{aligned} a &= \frac{u_{\max} T}{2\pi} \\ u_{\max} &= \frac{\pi H}{T sh(kh)} \\ \left(\frac{2\pi}{T}\right)^2 &= g \cdot k \cdot th(kh) \end{aligned} \tag{3}$$

where T is the period of the wave, H is the height of the wave, h is the depth of the water, k is the number of waves, and g is the acceleration due to gravity.

For the scenario with combined wave–current interaction, the shear stress or flow velocity can be calculated by Equations (2) and (3) to preliminarily judge the scour initiation.

Another important aspect when investigating scour is the study of the scour resistance of soils, which are characterized by the critical flow velocity V_{c} or critical shear stress τ_{c}. Briaud [35] analyzed the results of EFA tests on sand and combined several tests with field data [36–38] to calculate critical shear stress based on the median grain size of sand. For cohesive soils, Briaud [30] recommended using the critical shear stress and the scour velocity obtained from EFA tests to predict the depth of erosion. However, the discrete nature of the soil parameters leads to different scour phenomena at different locations, and the above equation is empirical in nature.

2.2. Use of Solidified Soils as Scour Countermeasure

It is important to improve the scour resistance of the soil around the foundation to reduce scour. In recent years, engineers have been actively exploring more suitable means for scour protection [39], drawing on the experience of slope and shore protection projects to improve the composition structure, engineering performance, and scour resistance of scour protection measures through soil solidification technology [40,41]. In offshore wind turbine scour protection projects, soil solidification methods can be mainly divided into in situ solidification methods and ex situ solidification methods, depending on the construction techniques used. In situ solidification is designed to improve the scour resistance of the original soil by mixing the original soil with a solidifying material in the area to be protected and using a mixer to form a solidifying pile; this method requires no additional material input and has a low cost, but the soil around the fan foundation is required to react well with the solidifying agent. In ex situ solidification, a pre-configured solidified soil slurry is used; pumping equipment is needed to pump the slurry into the protection area, and the protective layer will be formed after slurry solidification to achieve the effect of scour protection. The advantage of using this method is that there are no additional requirements based on the nature of the site soil, and existing scour pits around the foundation can be

filled to restore the seabed elevation around the foundation to the design level to achieve the effect of scour pit repair (but this requires a certain amount of soil suitable for the reaction of the solidifying agent as raw material). A schematic diagram of the solidified soil protection model is shown in Figure 3.

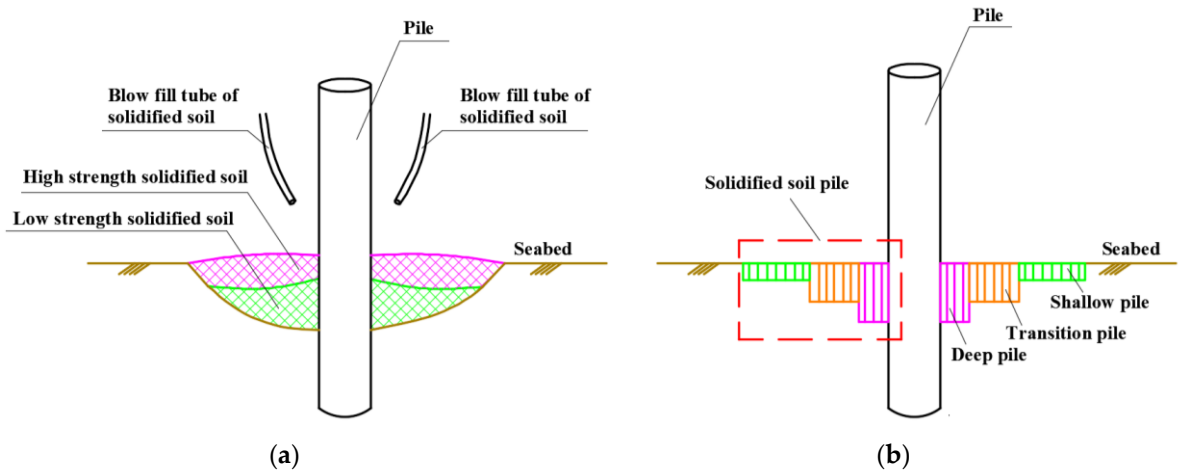

Figure 3. Schematic diagram of solidified soil protection. (**a**) In situ solidification (**b**) Ex situ solidification.

Soil solidification technology is a new form of scour protection for offshore wind turbine foundations. With its easy construction, good quality control, and good environmental protection, this technology has shown great potential for application in offshore wind turbine projects. However, there is no unified design standard for solidified soil as a scour protection technology for wind turbine foundations. As the design relies heavily on tests conducted in indoor laboratories and on engineering experience, the relevant theory for soil solidification for OWTs lags behind that for other applications, and the reliability during the entire service period of the OWT has to be demonstrated. This paper aims to establish the relationship between the UCS of the solidified soil and its scour resistance through the unconfined compression test and simplified scour resistance test in order to provide a reference for engineering design optimization of OWT scour protection measures.

3. Experimental Setup and Procedure

3.1. Soil Samples and Testing Groups

Soil samples retrieved from the construction site of a project were used for the experiment, and the soil sample type was gray silty clay of Shanghai layer ④ [42]. Through indoor geotechnical tests, the basic physical and mechanical parameters were determined as shown in Table 1. The soil retrieved from the construction site was dried in a dry and ventilated location for natural air-drying, as shown in Figure 4. In order to evenly mix the soil sample with cement powder and reduce the dispersion in the test results, the test soil sample was crushed using a crusher, and the crushed, air-dried soil powder was sealed and stored in a bucket for subsequent testing.

Table 1. Basic properties of silty clay in the ④ layer in Shanghai [33].

Moisture Content (%)	Density (g/cm^3)	Pore-Solid Ratio	Liquid Limit	Plastic Limit	UCS (kPa)
36.0~49.7	1.64~1.79	1.12~1.67	34.4~50.2	19.0~26.0	42~77

Cement is the main cementing component of the common solidification agent; through a reaction between the cement and soil, cement forms between soil pores to achieve a solidified soil. The appropriate type of cement should be selected based on the project. Sulphate aluminum cement has excellent characteristics, such as early strength, high strength, and resistance to sulfate erosion, as compared to ordinary silicate cement. The

early strength characteristic can effectively reduce the solidification time under the premise of guaranteeing the strength and, thus, the test time can be shortened. Sulphate aluminum cement's resistance to sulfate erosion can reduce the chemical erosion of the solidified soil in a marine environment. At the same time, the CO_2 generated during the production of sulfate aluminate is 40% less than that for ordinary silicate cement [43], which is more advantageous under current carbon emission policies. Considering the above factors, No. 425 sulphate aluminum cement was selected as the solidification material for the tests in the present study; the basic parameters of this cement are shown in Table 2. The cement was kept in a cool and dry place to prevent moisture from affecting the performance of the cement.

Figure 4. Air-drying of the soil.

Table 2. Parameters for the No. 425 sulphate aluminate cement used for testing.

Main Components	Rank	Specific Surface Area (m^2/kg)	UCS (MPa)		Solidified Age (min.)	
			1-Day	3-Day	Initial	Final
Sulphate, aluminate	425	≥350	30	42.5	15	30

In this paper, two types of tests were carried out: an unconfined compressive test to determine the geotechnical parameters of the soil and a SSRT test to reflect the scour resistance of the soil. The UCS is a common measure of the strength of solidified soil in engineering, as its testing principle is simple and the cost of testing is low. However, for offshore wind turbine scour protection projects, it is more important to test the scour resistance of the solidified soils. Soil scour resistance testing is not currently popular in engineering practice and is a complex and costly process. If the scour resistance can be estimated by the UCS, it can make the design optimization of the solidified soil scour protection project more convenient. At the same time, establishing the relationship between the UCS and the scour resistance of solidified soil can lay the foundation for studying the micro-scale mechanical mechanism that determines the scour resistance of the solidified soil. Therefore, in this paper, the unconfined compressive strength of the solidified soil was first determined by unconfined compression tests using soils with different cement contents. Next, the scour resistance performance, such as the scour critical flow velocity of the solidified soil under the corresponding UCS, was measured according to the ratio relationship obtained from the test. Finally, the relationship between the UCS and the scour resistance performance of the solidified soil was established.

Engineering practice shows that solidified soil that has a UCS above 400 kPa is able to achieve a better scour protection effect; therefore, in this test, the strength range of solidified soil is selected as 50~400 kPa. A silt soil with a high moisture content (70–80%) was selected for this test. In engineering practice, the water–cement ratio used to configure the solidified soil is generally determined based on the water content of the soil before solidification to ensure the final strength and compatibility of the solidified soil. If the water content of the soil itself is high, no additional water is added. Thus, the water content of the solidified soil

after solidification was controlled to 75% in this study, which is close to the water content of the raw soil itself. Based on the measurements made prior to the experiment, it was determined that the UCS of the solidified soil was 400 kPa at a moisture content of 75% and a cement admixture of approximately 30%. Therefore, the admixture of the solidified soil for this test was varied from 5% to 30%. Table 3 shows the test conditions for each group in the testing scheme for UCT.

Table 3. UCT testing scheme for the solidified soil.

Group *	Soil-to-Cement Ratio	Moisture Content of Solidified Soil	Solidified Age
U1	5%	75%	7 days
U2	10%	75%	7 days
U3	15%	75%	7 days
U4	20%	75%	7 days
U5	25%	75%	7 days
U6	30%	75%	7 days

* Three parallel tests, namely, T1, T2 and T3, for each group.

In order to establish a link between the UCS and the scour resistance, the strength of the solidified soil was selected to range between 50 kPa and 400 kPa to establish a link with the unconfined compression test. At the same time, the solidification time of the solidified soil has a great influence on its scour protection effect; thus, two states of solidification (initial setting and final setting) were considered in the test. The test conditions are shown in Table 4.

Table 4. SSRT testing scheme for the solidified soil.

Group	Targeted UCS (kPa)	Solidification States
S0	control group	no curing
S1, S2	50	initial setting, final setting
S3, S4	100	initial setting, final setting
S5, S6	150	initial setting, final setting
S7, S8	200	initial setting, final setting
S9, S10	300	initial setting, final setting
S11, S12	400	initial setting, final setting

3.2. Unconfined Compression Test

The unconfined compression test (UCT) is a special case of the triaxial compression test where no confining pressure is applied to a cylindrical soil sample, but only vertical axial pressure is applied, and the lateral direction is not restricted during the test, making it suitable for cohesive soils, especially saturated soft cohesive soils. The UCS of cohesive soils can be calculated using the UCT results. For cohesive soils or cohesive materials, the unconsolidated undrained strength is equal to half of the UCS. The UCT is widely used in engineering practice because it requires only simple equipment, it is easy to conduct, and the test can be conducted under controlled conditions. The UCS test in this study was carried out according to the "Specification for mix proportion design of cement soil" (JGJ/T 233-2011) [44] and the "Standard for geotechnical testing method" (GB/T 50123-2019) [45].

The UCT is divided into the following steps: (1) soil, cement, and water are mixed together to obtain a solidified soil slurry according to the ratio designed according to the working conditions. (2) The configured slurry is poured into cylindrical moulds with a height of 100 mm and a diameter of 50 mm in two to three layers, and the slurry is pounded with a pounding stick after pouring each layer to ensure that the specimen is uniform and free of air bubbles (as shown in Figure 5). The mould is then sealed with plastic film and is maintained at room temperature for 1 day. After the specimen has been removed from the mould, it is maintained in a standard maintenance room until Day 7. (3) The solidified soil samples are placed on the loading table for loading, and the corresponding axial stress

is recorded every 0.5% of the axial strain and the peak stress is recorded. The average for three specimens of each type is reported for each group of tests.

(**a**) (**b**)

Figure 5. Preparation of specimens for unconfined compression tests. (**a**) Cylindrical moulds (**b**) Specimens in the curing room.

3.3. Simplified Scour Resistance Test

In this study, the critical scour resistance velocity of solidified soil samples was determined using an SSRT device proposed by Wang et al. [31], and the corresponding critical shear stress was calculated. In a previous study, the authors investigated the scour resistance of sand with different individual and mixed grain sizes using the SSRT test equipment to analyze the effect of grain size and grading on the scour resistance of sand, and the test results obtained in that study were used to propose a method for calculating the scour critical flow velocity considering the grain size and grading. At the same time, Wang et al. [31] tested the scour resistance of Toyoura sample using SSRT equipment and compared the results with those of other researches to verify the reliability of the SSRT. However, the study was only conducted for sand, not for solidified soils.

During the SSRT test, the flow velocity at the soil–water interface at the axis of the cylindrical soil sample is less than that at the edge of the soil, and the erosion produced by the soil at different distances from the axis is different because the soil sample was uniform and the scour resistance was consistent [31]. As shown in Figure 6, point C is the observed dividing point between the non-erosion area and the erosion area; areas AC′ and CB are the erosion zones, while C′OC is the non-erosion area. According to the correspondence between the critical shear velocity and the speed of the blade in the test device, it is known that at point C, the critical shear velocity is equal to the tangential blade velocity. Thus, by observing the non-erosion area, the critical shear velocity can be calculated using the following expression:

$$V_c = \frac{n\pi l}{30} \tag{4}$$

where V_c is the critical shear velocity, l is the radius of the non-erosion area, and n is the rotation speed. It is worth noting that SSRT does not involve the simulation of complex hydraulic conditions (e.g., currents, waves, tides or their combinations) as is usually considered in macroscopic studies. The generated flow field is used to create a linear distribution of the flow velocity at the water–soil interface as well as to evaluate the scour resistance of soil samples when considering different stabilization conditions.

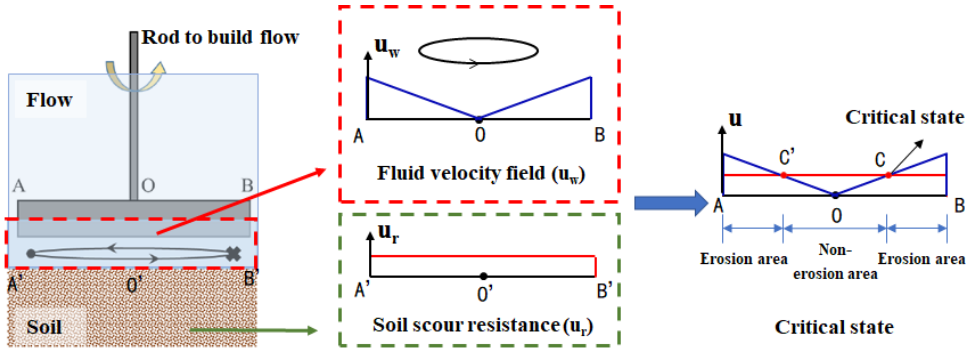

Figure 6. Erosion zone and non-erosion zone division in the simplified scour resistance test.

Engineering practice shows that the critical flow velocity for solidified soil is much larger than that for sand, and the velocity of water flow generated by the original equipment is not sufficient for the erosion of solidified soil. Therefore, certain modifications were made to the original equipment to increase the simulated flow velocity and enhance the stability of the equipment. The erosion flow field simulation portion of the improved SSRT equipment mainly includes the motor, speed control system, aluminum frame, and mixing head. The aluminum frame ensures the device will remain stable during operation, and the speed control system is used to adjust the flow velocity for different flow fields. A stirring head is designed to ensure that the fluid velocity field at the water–soil interface is linearly distributed with the radius range, the edge effect is reduced, and the stiffness is increased. The water tank and soil sample box are detachable to allow the soil samples to be prepared and replaced more easily, and graduation marks on the inner and outer surfaces of the tank are used to observe the liquid level and soil sample erosion during the test. A schematic diagram of the device is shown in Figure 7.

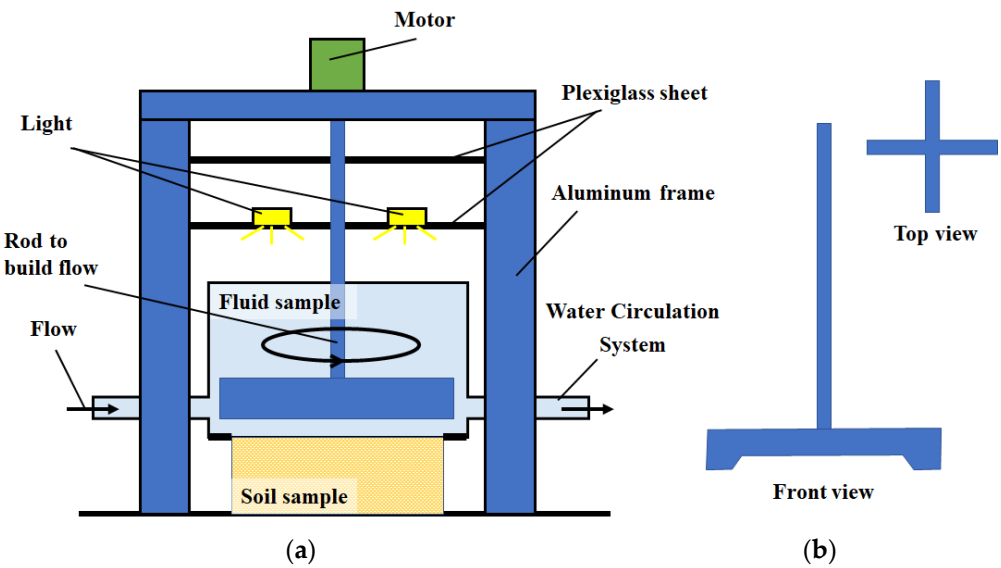

Figure 7. The schematic diagram of the SSRT device. (**a**) SSRT device (**b**) Stirring rod.

The simplified scour resistance tests in this study were conducted according to the following steps: (1) Prepare a test soil sample that is 20 mm height for each soil sample to be tested and place it in a test container with an outer diameter of 200 mm (as shown in Figure 8a,b), and slowly fill the container with water to saturate the sample; (2) adjust the power and control device of the instrument to simulate the erosion process of the soil under a certain flow range and vortex conditions (as shown in Figure 8c); (3) record the beginning of erosion, the maximum erosion depth of the soil sample, and the time required to reach

equilibrium; and (4) repeat the above process to complete the test of scour resistance under different unconfined compressive conditions.

(**a**) (**b**) (**c**)

Figure 8. Photographs of simplified scour resistance tests. (**a**) Top view of specimen (**b**) Side view of specimen (**c**) Activation of erosion simulator.

4. Results and Discussion

4.1. Unconfined Compression Test Results

Figure 9 presents images of typical damaged specimens from the unconfined compression tests. When the UCS is below 200 kPa, the damage presents in the form of a large main crack. When the UCS of the specimen is reached, a large main crack forms in the specimen, with a crack angle that is usually between 45° and 60°. When the UCS is above 200 kPa, a damage cone with an angle of approximately 45° typically forms at the top of the specimen; as the loading continues, an obvious crack forms under the action of the damage cone once the specimen reaches its limit.

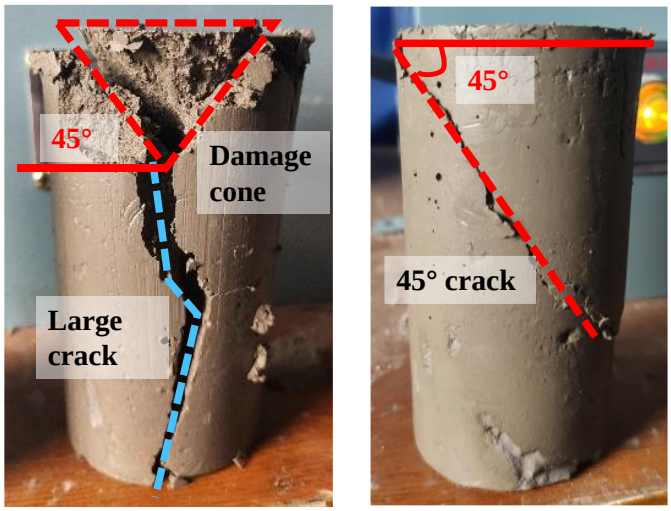

(**a**) (**b**)

Figure 9. Failure modes for UCT specimens. (**a**) Triangular damage cone (**b**) Major crack.

A summary of the UCT test results is shown in Figure 10. It is noted that the UCT results for the 10% cement admixture group are smaller than those of the 5% cement admixture group, but the difference in the results is not significant. The reason for this may be that when the cement admixture is small, the reinforcement effect is not obvious; moreover, the range of the dynamometer used for measuring the force per unit area is less accurate for specimens with lower strength. On balance, the effect of the 10% cement admixture should be retained when fitting the results to a group of test results.

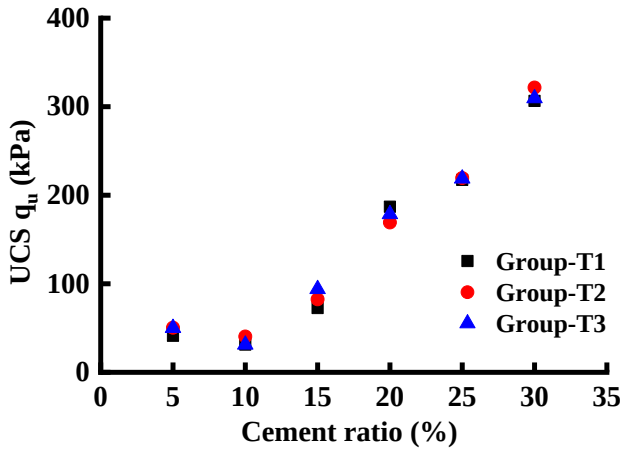

Figure 10. Summary of results of the unconfined compression tests.

If the error of the results of three parallel tests relative to the mean is within three times the standard deviation, the mean of the three tests is taken as the final result of the group of tests; otherwise, the group of tests is conducted again. The average UCS at each cement admixture was plotted in Figure 11. From this figure, it can be seen that the UCS grows slowly when the cement dosing is less than or equal to 15%; when the cement dosing exceeds 15%, the UCS of the solidified soil has an obvious rising trend with the increase in cement dosing. The UCS increases with the growth of cement admixture, and presents the characteristics of a slow growth in the early stage and a fast one in the late stage. The power function curve was used to fit the test results as shown in Figure 11.

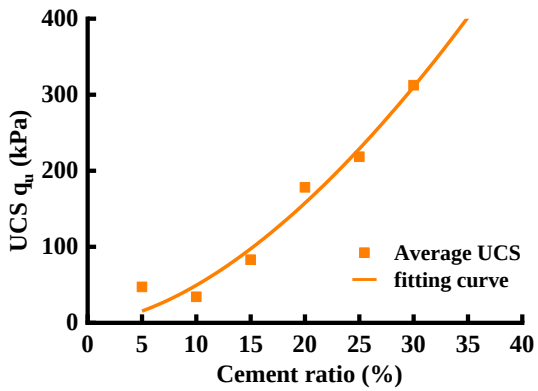

Figure 11. Relationship between the UCS of the solidified soil and the cement content.

Regression analysis of the test results was performed using a power function, and the strength-doping equation was obtained as shown in Equation (5).

$$q_u = 1.049 w_c^{1.673} \quad \text{(kPa)} \tag{5}$$

where w_c is the cement content (%). The calculated coefficient of determination R^2 is 0.9670; as this coefficient is greater than 0.95, the reliability of the regression results is considered to be high.

Jia [46] defined the integrated water content of the solidified soil as the ratio of water mass to solid mass (soil and cement) in the configuration of the solidified soil, and his research results showed that the integrated water content of the solidified soil has a great influence on the strength of the solidified soil at the same admixture dosage. The research in Jia's thesis was conducted for saturated soft clay soils in Shanghai, and the strength of solidified soil was found to reach the highest level when the integrated water content was approximately 30%. A water content that is too low will not meet the water requirement for a hydration reaction, and the strength will be reduced; a water content that is too high

will affect the crystallization reaction, making the content of cementitious material in the solidified soil lower and, thus, reducing the strength. At this stage of the study [37], the consideration of water content is mainly based on the natural moisture content of the actual topsoil and the fluidity of the solidified soil, which is high (thus, the strength is low). Consideration should be given to reducing the overall moisture content of the solidified soil without changing the fluidity in order to reduce the amount of cement needed. In particular, it is recommended to reduce the water content before mixing the solidified soil in order to more efficiently and economically improve the strength of the solidified soil during actual engineering operations.

4.2. Simplified Scour Resistance Test Results

After the solidified soil sample reaches erosion equilibrium, the water tank sample box is lowered from the platform, drained, and removed. Photographs were taken to record the surface morphology of the solidified soil after erosion, and the final erosion radius of the solidified soil and the erosion depth at each representative location were measured. Figure 12 shows the results of two typical post-erosion tests. During the tests, the water velocity at the surface of the soil sample is greater at locations farther away from the axis, so the erosion of the soil sample decreases as the distance from the axis decreases until it is less than the scour resistance of the soil sample and no further erosion occurs, forming a dividing line between areas with erosion and no erosion. The eroded soil and the water mixed with the water in the tank form a suspension due to the small size of the particles, which cannot accumulate at the axis where the flow velocity is low and is lost with the renewal of the test water; this process is different from the study for sand [31].

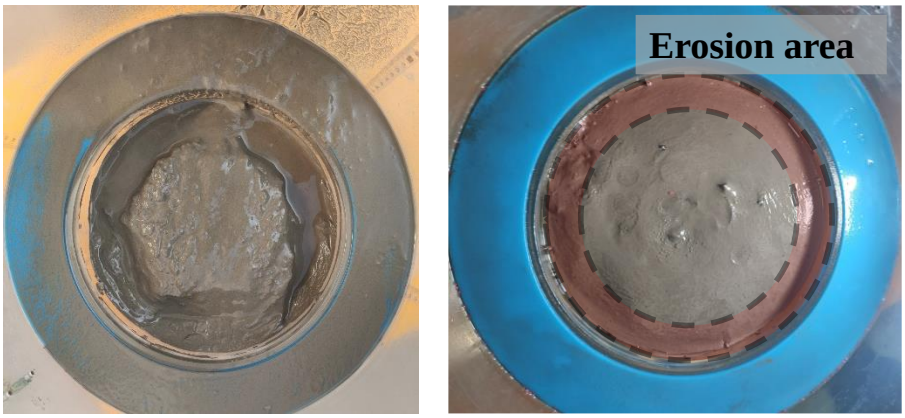

(**a**) (**b**)

Figure 12. Typical test results obtained from simplified scour resistance tests. (**a**) Low strength solidified soil (**b**) High strength solidified soil.

As can be seen in Figure 12, the erosion of solidified soils is more obvious for solidified soils with a shorter setting time and a lower strength. As the bond between soil particles has not yet developed completely, the erosion is deep. When the flow velocity becomes greater than the critical flow velocity, the erosion of the soil develops violently and the erosion rate is high, but it can typically reach equilibrium within a very short period of time. Low strength and a short solidification time for the solidified soil due to the degree of intense erosion causes the eroded soil particles to mix with water to form a high concentration of suspension. This increases the shear stress between the water and soil surface, thus intensifying the erosion phenomenon and increasing the depth and volume of erosion, which causes an area of the soil to become completely eroded. The unflushed soil does not collapse to the edge due to the balance of turbidity and soil pressure but rather forms an upright boundary between the flushed and non-flushed areas. For the solidified soil with a long solidification time and high strength, even though the flow velocity is greater than the critical flow velocity, the erosion rate is small, the rate of development of the erosion

depth is slow during the test, and it takes a long time for the system to reach the erosion equilibrium. At this time, the bond between soil particles has already formed (unlike the suspension that forms when a low-intensity, short-time solidified soil is eroded vigorously), the concentration of suspension in the test is low, the exacerbating effect on erosion is smaller, and the surface of the soil sample transitions gently from the non-erosion area to the erosion area. The results for each test group are plotted in the cloud diagrams shown in Figures 13 and 14.

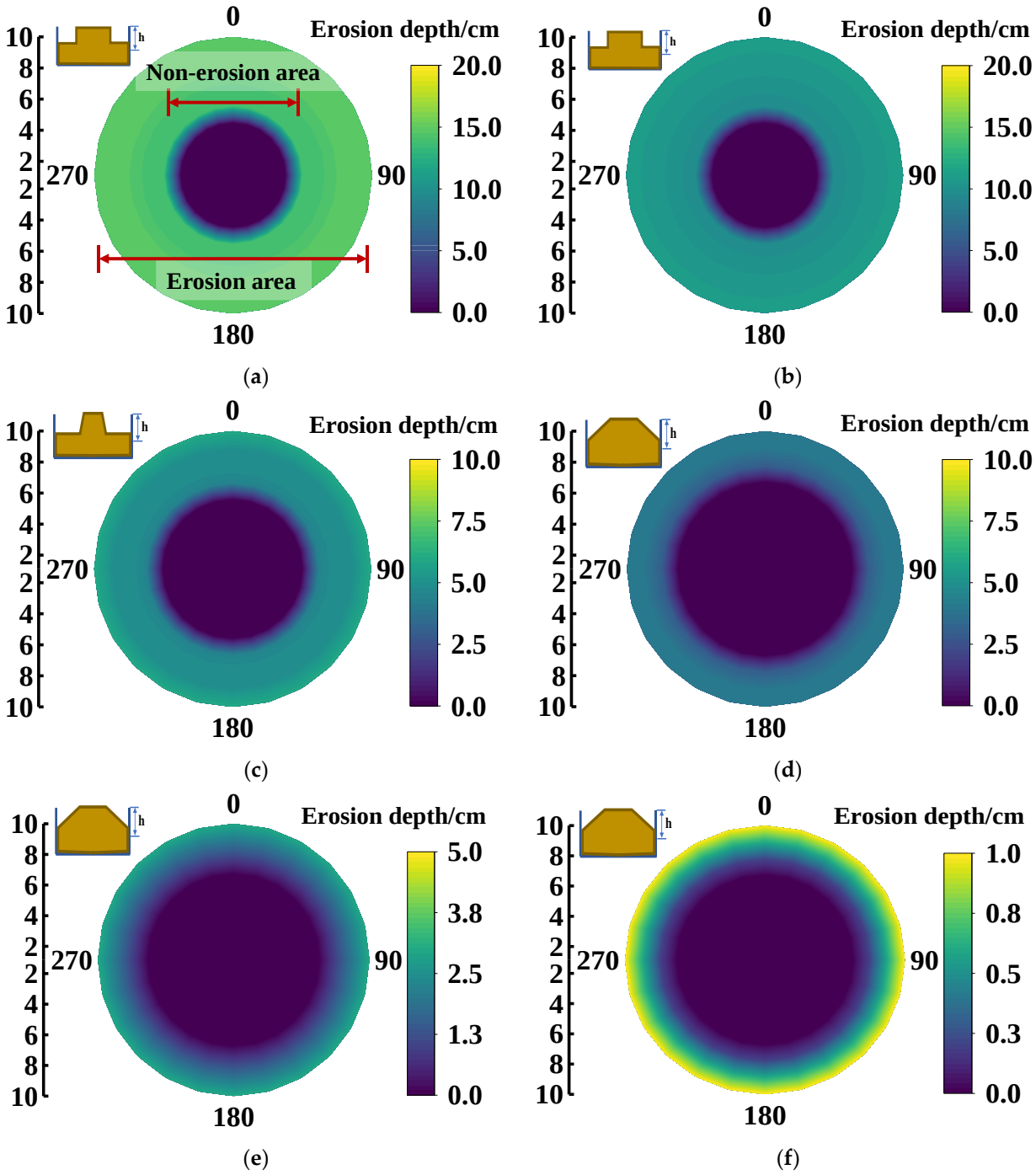

Figure 13. Erosion topography map for each test condition (initial setting). (**a**) 50 kPa (w = 60 rad/s) (**b**) 100 kPa (w = 50 rad/s) (**c**) 150 kPa (w = 90 rad/s) (**d**) 200 kPa (w = 100 rad/s) (**e**) 300 kPa (w = 131 rad/s) (**f**) 400 kPa (w = 153 rad/s).

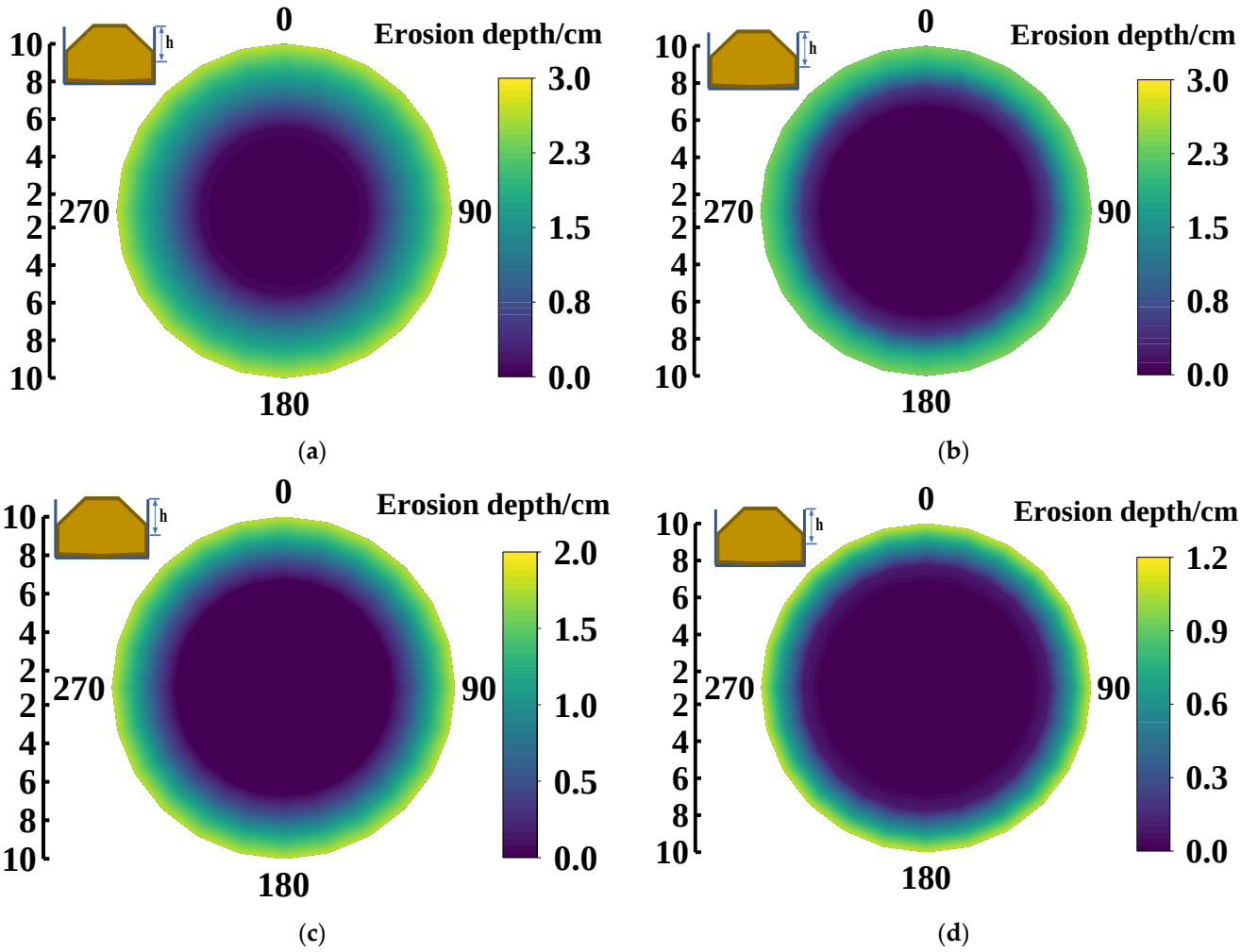

Figure 14. Erosion topography map for each test condition (final setting). (**a**) 50 kPa (w = 124 rad/s) (**b**) 100 kPa (w = 123 rad/s) (**c**) 150 kPa (w = 156 rad/s) (**d**) 200 kPa (w = 201 rad/s).

By observing the surface changes of the solidified soil samples during erosion, the process of solidified soil erosion development can be roughly divided into the following stages: initial formation of the cracks (Figure 15a), gradual development and extension of the cracks (Figure 15b) and, after the final formation of the erosion line, the rapid erosion of the local solidified soil mass at the corresponding location within a relatively short period of time (Figure 15c). This phenomenon is obviously different from the "uniform" erosion of sand. When the partially solidified soil is separated from the rest of the soil sample, it will be rapidly broken into fine particles that become suspended in the water to form turbidity, resulting in the gradual increase in turbidity of the water in the tank. As the erosion depth becomes greater, the hydraulic action on the deep soil decreases, and the erosion eventually reaches equilibrium, as shown in Figure 15d. For solidified soil in the initial setting, the water flow can push the solidified soil at the soil surface from one side to the other (Figure 15a), making it easier to create cracks and thus make the soil more susceptible to erosion. In contrast, the final consolidated soil cannot be pushed, so erosion is difficult.

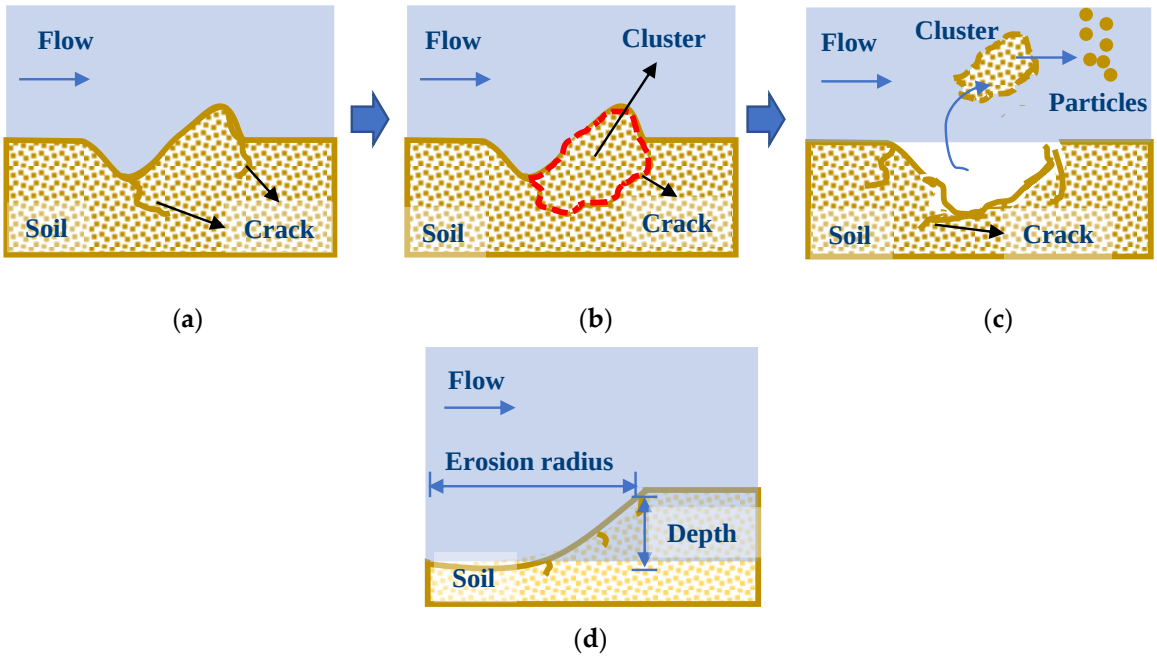

Figure 15. Evolution of erosion of solidified soil (initial setting). (**a**) Erosion line formation (**b**) Erosion line extension/penetration (**c**) Local intense erosion (**d**) Erosion equilibrium.

4.3. Relationship between Scour Resistance and Solidified Soil UCS

Unlike sand, where individual particles are scoured, solidified soil is eroded mostly in the form of clusters or flakes, showing the process of cracking → expansion → penetration → destruction. Thus, the scour resistance of solidified soil should include the cohesion between soil particles in addition to the self-weight of the particles and the forces due to friction, which are related to geotechnical properties, such as the stress history, shear strength indices (c, φ), and the plasticity index of the soil. The critical shear stress τ_{cr} of the scour resistance of the solidified soil should be generated by gravity W and the cohesion F between solidified soil clumps, as shown in Figure 16. According to the force analysis, the following equation can be obtained:

$$\tau_R \sim f[c, \varphi] \tag{6}$$

$$\tau_{cr} A = \sqrt{F^2 + W^2} \sim \sqrt{(\tau_R A)^2 + W^2} \tag{7}$$

where τ_R is the shear stress of the soil, c is the cohesion, φ is the internal angle of friction, W is the gravity of the soil clump, F is the cohesion between soil clumps, and A is the effective surface area of the soil cluster.

The shear strength index can be obtained by conducting triaxial tests, and the relationship between the positive stress σ_1, confining pressure σ_3, and the shear strength index in triaxial test can be expressed by Equation (8). For the UCT, the ultimate positive stress q_u is σ_1 and σ_3 is equal to 0. Therefore, Equation (8) can be converted to Equation (9).

$$\sigma_1 = \sigma_3 \tan^2(45^\circ + \frac{\varphi}{2}) + 2c \tan(45^\circ + \frac{\varphi}{2}) \tag{8}$$

$$c = \frac{q_u}{2\tan(45^\circ + \frac{\varphi}{2})} = Kq_u \tag{9}$$

where σ_1 is the positive stress, σ_3 is the confining pressure, c is the cohesion, φ is the internal angle of friction, and q_u is the UCS.

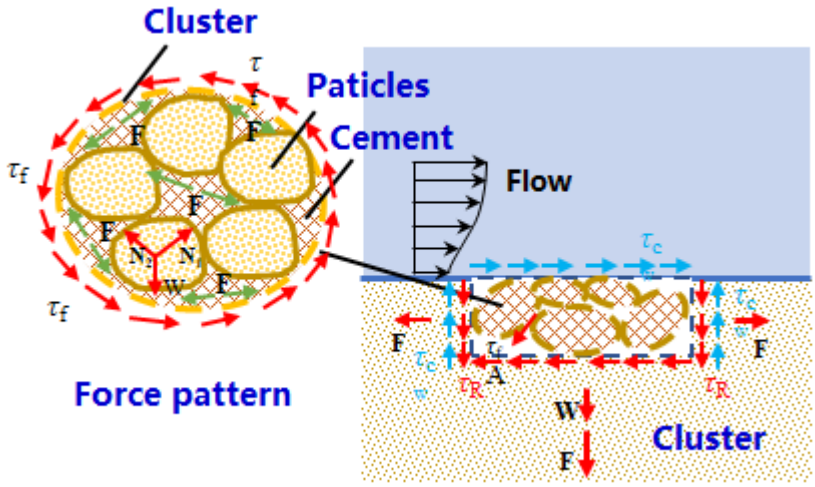

Figure 16. Schematic diagram of the water flow and the scour resistance of solidified soil during erosion.

Since erosion always occurs at the surface of the soil, the positive stress can be considered as 0, and the shear strength is only related to the cohesion; thus, the relationship between the UCS and the critical shear stress can be established, as shown in Equation (10):

$$\tau_{cr}A \sim \sqrt{(Kq_uA)^2 + W^2} \tag{10}$$

Since many calibration parameters are still needed to calculate the critical shear in Equation (10) and the critical scour flow velocity in SSRT is a direct test result, the relationship between the UCS and the critical flow velocity can be established first to prepare for further fine-scale analysis.

The relationship between UCS and the critical scour flow velocity is shown in Figure 17. The dashed line represents the experimental results for pure clay without any solidifying treatment (the same with Figures 18 and 19). Between 50 kPa and 400 kPa, the critical flow velocity of the solidified soil in the initial setting gradually tends to level off with the increase in strength; when the solidified soil is in the final setting, the critical flow velocity of the solidified soil continues to increase with the increase in strength. The power function model was used to fit the relationship between the UCS and the critical flow velocity.

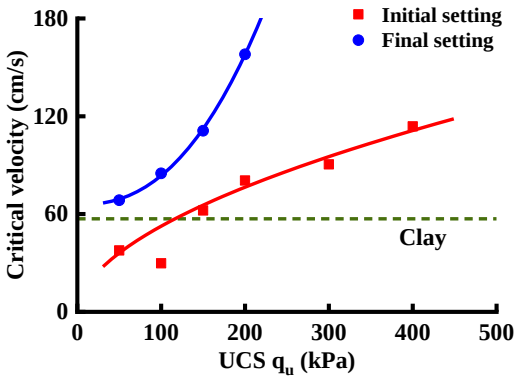

Figure 17. Relationship between the UCS and the critical flow velocity.

The relationship between the UCS and the equilibrium erosion depth is shown in Figure 18. The equilibrium erosion depth decreases with the increase of solidified soil strength. However, when the strength of solidified soil is greater than 150 kPa, the equilibrium erosion depth is already very small, the effect of increasing strength on decreasing depth is no longer obvious, and the equilibrium erosion depth gradually approaches a small value. A hyperbolic model was used to fit the relationship between the unconfined strength

and the equilibrium erosion depth. From Figure 18, it can be seen that for the solidified soil in the initial setting, the equilibrium erosion depth decreases significantly with the increase of strength; however, when the strength exceeds 200 kPa, the equilibrium erosion depth of the solidified soil is already below 5 mm, and the decrease in the equilibrium erosion depth of the solidified soil tends to level off gradually when the strength continues to increase. For the solidified soil in the final setting, even when the strength is 50 kPa, the equilibrium erosion depth is already below 5 mm. The erosion depth is less obvious with the change of strength in the later stages. When the strength reaches 300 kPa or more, no further erosion occurs under the conditions provided by the test.

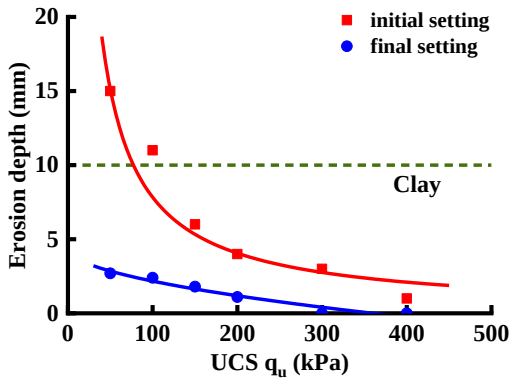

Figure 18. Relationship between the UCS and equilibrium erosion depth.

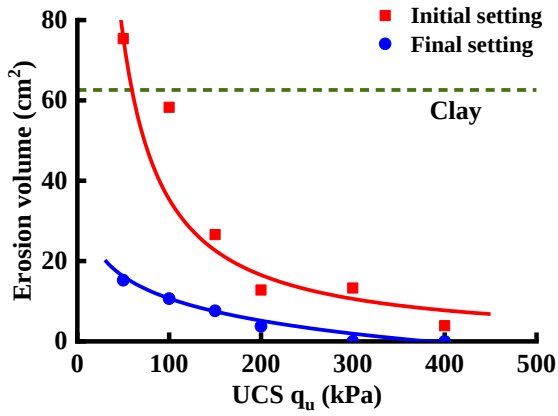

Figure 19. Relationship between the UCS and the volume of erosion.

In order to further investigate the loss of solidified soil during erosion, the volume of erosion during erosion for solidified soils of different strengths is calculated. The volume of solidified soil being eroded can be calculated by using the integral of the surface function of the terrain after erosion, as shown in Equation (11). According to the test, it is assumed that no accumulation occurs and that the solidified soil is discharged together with the turbidity. Further, to simplify the calculation, because the viscous material has a certain uprightness, the erosion area of the solidified soil is assumed to be a regular circle, the erosion depth is estimated according to the maximum value in the erosion range, and the estimated erosion volume of the solidified soil can be obtained as shown in Equation (12):

$$V = \frac{\pi D^2}{4} - \iint_S h(x,y)\mathrm{d}\sigma \tag{11}$$

$$V = \frac{\pi}{4}(D^2 - D_{cr}^2)h_{\max} \tag{12}$$

where V is the volume of erosion (cm^3), $h(x,y)$ is the topographic function after erosion (cm), S is the erosion area (cm^2), D is the soil sample box radius (cm), D_{cr} is the erosion critical radius (cm), and $h_{\max}$ is the maximum erosion depth (cm).

The relationship between the UCS and the erosion volume calculated using Equation (12) is shown in Figure 19. From Equation (12), it can be noticed that the erosion volume of the solidified soil is a combination of the effects of the erosion radius and the erosion depth, reflecting a comprehensive law for solidified soil erosion. Similar to the variation rule of equilibrium erosion depth with strength, the effect of an increase in strength on the amount of solidified soil loss is greater in the early stages of erosion, and it gradually becomes stabilized in the later stages. Therefore, the selection of solidified soil strength should take into account the material cost of high strength and the loss cost of low strength. The fitting relationship of strength vs. the volume of erosion is similar to that for strength vs. equilibrium erosion depth, which shows a hyperbolic relationship (see the fitting curve in Figure 19). As the strength increases, the decrease in the curve tends to level off, and the amount of solidified soil that is eroded approaches or even reaches zero.

The above fitting results are summarized in Table 5. The coefficients of determination of the regression analysis, R^2, are all above 0.95, indicating that the fitted formulas have high reliability for the experimental results.

Table 5. Relationship between the UCS and each soil scour resistance performance index.

Relationship	Solidified State	Formula (Units)	R^2 Value
UCS vs. critical flow velocity	Initial	$v_c = 4.359{q_u}^{0.5407}$ (cm/s)	0.9822
	Final	$v_c^t = 0.0003{q_u}^{2.37} + 65.72$ (cm/s)	0.9991
UCS vs. equilibrium erosion depth	Initial	$d = 618.8{q_u}^{-0.9489}$ (mm)	0.9854
	Final	$d^t = -0.1775{q_u}^{0.5428} + 4.334$ (mm)	0.9504
UCS vs. erosion volume	Initial	$V = 5526{q_u}^{-1.097}$ (cm^3)	0.9842
	Final	$V^t = -1934{q_u}^{-0.0040} + 1981$ (cm^3)	0.9770

5. Conclusions

With the rapid development of offshore wind power farms, the problem of local scour of the OWT foundation has received increasing attention from engineers and researchers. Most wind power foundations adopt a large diameter monopile foundation, which is more likely to cause a greater degree of local scour, resulting in turbine instability, a drop in self-oscillation frequency, and other problems. Therefore, it is necessary to adopt local scour protection measures. Solidified soil scour protection has the advantages of environmental protection, good integrity, and strong scour resistance, and it is being applied in an increasing number of scour protection projects for offshore wind turbine foundations. However, there are few relevant studies to support the design of the solidified soils as scour countermeasures of OWTs. In this paper, an SSRT device developed by the authors was used to study the scour resistance of solidified soil. First, a UCT was carried out to test the UCS of the solidified soil with different cement admixtures at natural water content. After obtaining the development pattern for the UCS of solidified soil with a cement admixture, the critical flow velocity of the solidified soil against erosion at different UCS levels was tested. Based on the test results, the following conclusions can be made:

- The development pattern for the UCS of solidified soil containing a cement admixture can be approximated by fitting a power function. The fitted results can be used to estimate the UCS of solidified soils at the corresponding admixture levels;
- The direct solidification of natural soil with a high moisture content can ensure compatibility during construction, but the UCS is small. In engineering practice, for the solidification of silt with a high moisture content, water reduction measures should be considered to reduce the moisture content of the silt soil and to reduce the required amount of cement;
- The critical flow velocity, equilibrium erosion depth, and equilibrium erosion volume of the solidified soil are several parameters used to measure the scour resistance of the solidified soil, and these can be determined by conducting SSRTs. The fitted relationship between the parameters for scour resistance and the UCS can be obtained

as shown in Table 5. In the initial setting state, the critical scour velocity of the solidified soil grows with the UCS, and the growth slows when the UCS is above 300 kPa. In the final setting state, the critical flow velocity of scouring of the solidified soil increases rapidly with the growth in UCS, and the critical flow velocity is above 3.14 m/s when the UCS is above 300 kPa;

- In the strength range of the test design, the critical scour velocity of the initial solidified soil tends to level off with increasing strength, while the critical scour velocity of the final solidified soil increases significantly with increasing strength. The test results show that the solidification state of the solidified soil has a great impact on its scour resistance, and the critical scour velocity of the final solidified soil increases by 80% to 150% as compared to the initial solidified soil at the same strength.

Overall, the scour resistance of the solidified soil is much higher than that of natural clay or sand. When fully set, its scour resistance can cope with the conventional and extreme conditions faced by offshore wind power foundations, and the safety and reliability will also be higher. It should be noted, however, that during the pumping (or curing soil mixing pile construction) → fill completion → continuing to solidify after filling → consolidation completion, the solidified soil is susceptible to water erosion and loss, and a certain amount of tolerance should be considered during construction. The specific law is subject to further experimental research.

Author Contributions: Conceptualization, J.W., J.X. and Y.W.; methodology, J.W. and C.W.; validation, F.L. and C.W.; investigation, Y.W.; resources, J.W. and J.X.; data curation, Y.W. and J.W.; writing—original draft preparation, Y.W. and J.W.; writing—review and editing, C.W. and F.L. All authors have read and agreed to the published version of the manuscript.

Funding: This research was funded by Guangxi Key Laboratory of Geomechanics and Geotechnical Engineering (No. 20-Y-KF-07) and the Research Project funded by CCCC Third Harbor Engineering Co., Ltd.

Institutional Review Board Statement: Not applicable.

Informed Consent Statement: Not applicable.

Data Availability Statement: Data available on request due to restrictions eg privacy or ethical. The data presented in this study are available on request from the corresponding author.

Acknowledgments: This work was supported by Guangxi Key Laboratory of Geomechanics and Geotechnical Engineering (No. 20-Y-KF-07), and the Research Project funded by CCCC Third Harbor Engineering Co. Ltd. Financial support from these organizations is gratefully acknowledged.

Conflicts of Interest: The authors declare no conflict of interest.

References

1. Lee, J.; Zhao, F. *GWEC Global Wind Report*; Global Wind Energy Council: Brussels, Belgium, 2022; p. 75.
2. Lizet, R.; Daniel, F.; Guy, B.; O'Sullivan, R. Offshore Wind in Europe—Key Trends and Statistics 2020. *Wind Eur.* **2021**, *3*, 14–17.
3. Bhattacharya, S. Challenges in Design of Foundations for Offshore Wind Turbines. *Eng. Technol. Ref.* **2014**, *1*, 922. [CrossRef]
4. Wang, C.; Yu, X.; Liang, F. A Review of Bridge Scour: Mechanism, Estimation, Monitoring and Countermeasures. *Nat. Hazards* **2017**, *87*, 1881–1906. [CrossRef]
5. Melling, G.J. Hydrodynamic and Geotechnical Controls of Scour around Offshore Monopiles. Ph.D. Thesis, University of Southampton, Southampton, UK, 15 June 2015.
6. Bennett, C.R.; Lin, C.; Parsons, R.; Han, J. Evaluation of Behavior of a Laterally Loaded Bridge Pile Group under Scour Conditions. In Proceedings of the Structures Congress 2009: Don't Mess with Structural Engineers: Expanding Our Role, Austin, TX, USA, 30 April–2 May 2009; pp. 1–10.
7. Lin, C.; Han, J.; Bennett, C.; Parsons, R.L. Behavior of Laterally Loaded Piles under Scour Conditions Considering the Stress History of Undrained Soft Clay. *J. Geotech. Geoenviron. Eng.* **2014**, *140*, 6014005. [CrossRef]
8. Liang, S.; Zhang, Y.; Yang, J. An Experimental Study on Pile Scour Mitigating Measures under Waves and Currents. Sci. *China Technol. Sci.* **2015**, *58*, 1031–1045. [CrossRef]
9. Liang, F.; Liang, X.; Zhang, H.; Wang, C. Seismic Response from Centrifuge Model Tests of a Scoured Bridge with a Pile-Group Foundation. *J. Bridg. Eng.* **2020**, *25*, 4020054. [CrossRef]

10. Liang, F.; Yuan, Z.; Liang, X.; Zhang, H. Seismic Response of Monopile-Supported Offshore Wind Turbines under Combined Wind, Wave and Hydrodynamic Loads at Scoured Sites. *Comput. Geotech.* **2022**, *144*, 104640. [CrossRef]
11. Chiew, Y.-M. Mechanics of Riprap Failure at Bridge Piers. *J. Hydraul. Eng.* **1995**, *121*, 635–643. [CrossRef]
12. De Vos, L.; De Rouck, J.; Troch, P.; Frigaard, P. Empirical Design of Scour Protections around Monopile Foundations: Part 1: Static Approach. *Coast. Eng.* **2011**, *58*, 540–553. [CrossRef]
13. Soulsby, R.L. Dynamics of Marine Sands: A Manual for Practical Applications. *Oceanogr. Lit. Rev.* **1997**, *9*, 947.
14. Esteban, M.D.; López-Gutiérrez, J.-S.; Negro, V.; Sanz, L. Riprap Scour Protection for Monopiles in Offshore Wind Farms. *J. Mar. Sci. Eng.* **2019**, *7*, 440. [CrossRef]
15. Isbash, S. Construction of Dams by Depositing Rock in Running Water. In *Transactions of the Scientific Research Institute of Hydrotechnics*; U.S. Engineering Office, War Department: Kansas City, MO, USA, 1935; pp. 66–76.
16. *DNV Offshore Standard DNV-OS-J101*; Det Norske Veritas. Design of Offshore Wind Turbine Structures. DNV AS: Høvik, Norway, 2014.
17. Sumer, B.M.; Fredsøe, J.; Christiansen, N. Scour around Vertical Pile in Waves. *J. Waterw. Port Coast. Ocean Eng.* **1992**, *118*, 15–31. [CrossRef]
18. Myrhaug, D.; Chen Ong, M. Effects of Sand-Clay Mixtures on Scour around Vertical Piles Due to Long-Crested and Short-Crested Nonlinear Random Waves. *J. Offshore Mech. Arct. Eng.* **2013**, *135*, 034502. [CrossRef]
19. Corvaro, S.; Marini, F.; Mancinelli, A.; Lorenzoni, C.; Brocchini, M. Hydro-and Morpho-Dynamics Induced by a Vertical Slender Pile under Regular and Random Waves. *J. Waterw. Port Coast. Ocean Eng.* **2018**, *144*, 4018018. [CrossRef]
20. Sumer, B.M.; Fredsøe, J. Scour around Pile in Combined Waves and Current. *J. Hydraul. Eng.* **2001**, *127*, 403–411. [CrossRef]
21. Chen, B.; Li, S. Experimental Study of Local Scour around a Vertical Cylinder under Wave-Only and Combined Wave-Current Conditions in a Large-Scale Flume. *J. Hydraul. Eng.* **2018**, *144*, 4018058. [CrossRef]
22. Qi, W.-G.; Gao, F.-P. Physical Modeling of Local Scour Development around a Large-Diameter Monopile in Combined Waves and Current. *Coast. Eng.* **2014**, *83*, 72–81. [CrossRef]
23. Dong, X.; Lian, J.; Wang, H.; Yu, T.; Zhao, Y. Structural Vibration Monitoring and Operational Modal Analysis of Offshore Wind Turbine Structure. *Ocean Eng.* **2018**, *150*, 280–297. [CrossRef]
24. Zhang, R.; Zheng, S.; Zheng, J. Experimental Study on Strength Behavior of High Water Content Clay Stabilized by Low Amount of Cement. *J. Huazhong Univ. Sci. Technol. Sci. Ed.* **2015**, *43*, 101–106.
25. Li, X. Theoretical Study on Stabilization of Marine Soft Clay in Hangzhou. Ph.D. Thesis, Zhejiang University, Hangzhou, China, 2013.
26. Bell, F.G. An Assessment of Cement-PFA and Lime-PFA Used to Stabilize Clay-Size Materials. *Bull. Int. Assoc. Eng. Geol. l'Association Int. Géologie L'ingénieur* **1994**, *49*, 25–32. [CrossRef]
27. Al-Amoudi, O.S.B. Characterization and Chemical Stabilization of Al-Qurayyah Sabkha Soil. *J. Mater. Civ. Eng.* **2002**, *14*, 478–484. [CrossRef]
28. Horpibulsuk, S.; Rachan, R.; Chinkulkijniwat, A.; Raksachon, Y.; Suddeepong, A. Analysis of Strength Development in Cement-Stabilized Silty Clay from Microstructural Considerations. *Constr. Build. Mater.* **2010**, *24*, 2011–2021. [CrossRef]
29. Wang, D.; Zentar, R.; Abriak, N.E. Durability and Swelling of Solidified/Stabilized Dredged Marine Soils with Class-F Fly Ash, Cement, and Lime. *J. Mater. Civ. Eng.* **2018**, *30*, 4018013. [CrossRef]
30. Briaud, J.-L.; Ting, F.C.K.; Chen, H.C.; Gudavalli, R.; Perugu, S.; Wei, G. SRICOS: Prediction of Scour Rate in Cohesive Soils at Bridge Piers. *J. Geotech. Geoenviron. Eng.* **1999**, *125*, 237–246. [CrossRef]
31. Wang, C.; Yuan, Y.; Liang, F.; Yu, X.B. Investigating the Effect of Grain Composition on the Erosion around Deepwater Foundations with a New Simplified Scour Resistance Test. *Transp. Geotech.* **2021**, *28*, 100527. [CrossRef]
32. Maniatis, G.; Hoey, T.; Hodge, R.; Rickenmann, D.; Badoux, A. Inertial Drag and Lift Forces for Coarse Grains on Rough Alluvial Beds Measured Using In-Grain Accelerometers. *Earth Surf. Dyn.* **2020**, *8*, 1067–1099. [CrossRef]
33. Li, J.; Tao, J. CFD-DEM Two-Way Coupled Numerical Simulation of Bridge Local Scour Behavior under Clear-Water Conditions. *Transp. Res. Rec.* **2018**, *2672*, 107–117. [CrossRef]
34. Hong, D. The Experiment Study on the Scouring Characteristics of Cohesive Undisturbed Soil. Ph.D. Thesis, Hohai University, Nanjing, China, 2005.
35. Briaud, J.-L. Case Histories in Soil and Rock Erosion: Woodrow Wilson Bridge, Brazos River Meander, Normandy Cliffs, and New Orleans Levees. *J. Geotech. Geoenviron. Eng.* **2008**, *134*, 1425–1447. [CrossRef]
36. Briaud, J.-L.; Ting, F.C.K.; Chen, H.C.; Cao, Y.; Han, S.W.; Kwak, K.W. Erosion Function Apparatus for Scour Rate Predictions. *J. Geotech. Geoenviron. Eng.* **2001**, *127*, 105–113. [CrossRef]
37. White, C.M. The Equilibrium of Grains on the Bed of a Stream. *Proc. R. Soc. Lond. Ser. A Math. Phys. Sci.* **1940**, *174*, 322–338.
38. Vanoni, V.A. *Sedimentation Engineering*; American Society of Civil Engineers: Reston, VA, USA, 2006.
39. Tang, Z.; Melville, B.; Singhal, N.; Shamseldin, A.; Zheng, J.; Guan, D.; Cheng, L. Countermeasures for Local Scour at Offshore Wind Turbine Monopile Foundations: A Review. *Water Sci. Eng.* **2022**, *15*, 15–28. [CrossRef]
40. Kitazume, M.; Satoh, T. Development of a Pneumatic Flow Mixing Method and Its Application to Central Japan International Airport Construction. *Proc. Inst. Civ. Eng.-Ground Improv.* **2003**, *7*, 139–148. [CrossRef]

41. Morohoshi, K.; Yoshinaga, K.; Miyata, M.; Sasaki, I.; Saitoh, H.; Tokoro, M.; Fukuda, N.; Fujii, T.; Yamada, K.; Ishikawa, M. Design and Long-Term Monitoring of Tokyo International Airport Extension Project Constructed on Super-Soft Ground. *Geotech. Geol. Eng.* **2010**, *28*, 223–232. [CrossRef]
42. *China Standard DGJ08-37-2018*; Code for Investigation of Geotechnical Engineering. Shanghai Construction and Building Materials Industry Market Management Station: Shanghai, China, 2018.
43. Wang, Y. *Sulphoaluminate Cement*; Beijing University of Technology Press: Beijing, China, 1999.
44. *China Standard JGJ/T 233-2011*; Specification for Mix Proportion Design of Cement Soil. China Architecture Press: Beijing, China, 2011.
45. *China Standard GB/T 50123-2019*; Standard for Geotechnical Testing Method. China Planning Press: Beijing, China, 2019.
46. Jia, J. Research on Comprehensive Water Content of Cement Treated Soil. *Chin. J. Undergr. Space Eng.* **2006**, *2*, 132–136.